

"This accepted author manuscript is copyrighted and published by Elsevier. It is posted here by agreement between Elsevier and MTA. The definitive version of the text was subsequently published in [Ceramics International, 2018, 44, 22976-22982.; DOI 10.1016/j.ceramint.2018.09.096]. Available under license CC-BY-NC-ND."

Synthesis and characterization of Sr and Mg-doped hydroxyapatite by a simple precipitation method

Teodóra Nagyné-Kovács^{a,*}, Levente Studnicka^a, Annamária Kincses^b, Gabriella Spengler^b, Mónika Molnár^c, István Endre Lukács^d, Imre M. Szilágyi^a, György Pokol^{a,e}

^a *Department of Inorganic and Analytical Chemistry, Budapest University of Technology and Economics, Műegyetem rakpart 3., Budapest, H-1111, Hungary*

^b *Department of Medical Microbiology and Immunobiology, University of Szeged, Dóm tér 10., Szeged, H-6720, Hungary*

^c *Department of Applied Biotechnology and Food Science, Budapest University of Technology and Economics, Műegyetem rakpart 3., Budapest, H-1111, Hungary*

^d *Research Institute for Technical Physics and Materials Science, Hungarian Academy of Sciences, Konkoly Thege M. út 29-33, Budapest, H-1121 Hungary*

^e *Research Centre for Natural Sciences, Hungarian Academy of Sciences, Magyar tudósok körútja 2., Budapest, H-1117, Hungary*

**Corresponding author telephone number and e-mail: +36 1 463 1216, kovacs.teodora@mail.bme.hu*

ABSTRACT

This study presents the preparation of pure, Sr and Mg-doped hydroxyapatite (HAP) by precipitation. Sr-doped HAPs (SrHAPs) and Mg-doped HAPs (MgHAPs) were fabricated with Sr molar ratio of 2, 4, 6, 8, 12 % and Mg molar ratio of 2, 4 %, respectively. $\text{Ca}(\text{NO}_3)_2$, $\text{Sr}(\text{NO}_3)_2$, $\text{Mg}(\text{NO}_3)_2$, $(\text{NH}_4)_2\text{HPO}_4$ were used as starting materials, the Ca/P molar ratio was kept 1.67 during every synthesis and a 900 °C heat treatment was conducted to enhance the crystallinity. All of the products were analyzed by XRD, SEM and EDX, moreover lattice parameters and crystallite size calculations were performed to prove the ion incorporation into the crystal structure. The HAP structure was maintained when 2 and 4 Sr and 2 Mg % were applied and EDX confirmed the Sr and Mg content in these samples. In all other cases, various Sr and Mg-containing phases ($\text{Sr}_{0.13}\text{Ca}_{2.87}(\text{PO}_4)_2$, $\text{Ca}_2\text{P}_2\text{O}_7$, $\text{Mg}_{0.29}\text{Ca}_{2.71}(\text{PO}_4)_2$) were identified while the HAP structure disappeared. It was shown that lattice parameters and the unit cell volume of Sr-doped HAPs increased slightly compared to pure HAP due to the bigger radius of Sr^{2+} than Ca^{2+} . As the ionic radius of Mg^{2+} is smaller than Ca^{2+} , we demonstrated the distortion in the unit cell. Crystallite sizes increased as the amount of Sr and Mg raised. SEM experiments demonstrated that ion incorporation had little influence on the morphology, i.e. pure, Sr or Mg-doped HAPs were mostly homogenous, constituted of strongly sintered nanometer sized grains. Antimicrobial tests indicated that SrHAP with 4 Sr % and MgHAP with 2 % Mg had positive effect on cell viability.

KEYWORDS

Sr and Mg-doped hydroxyapatite, calcination, lattice parameters, crystallite size, antibacterial activity

1. Introduction

Natural hydroxyapatite (HAP, $\text{Ca}_{10}(\text{PO}_4)_6\text{OH}_2$) is an essential compound of hard tissues in vertebrates, forming the inorganic part of its matrix. In natural bones and teeth the inorganic material constitutes mostly of Ca^{2+} , PO_4^{3-} and OH^- ions, but others such as HPO_4^{2-} , CO_3^{2-} , Mg^{2+} , Na^+ , Zn^{2+} etc. can also be a part of the crystal structure of HAP through ion-substitutions [1–3].

Due to its physico-chemical similarity to the calcium phosphate based materials in natural hard tissues, synthetic HAP has attracted considerable interest in the past few decades. It possesses outstanding biocompatibility, non-toxicity and osteoconductivity which characteristics make it a potential material for orthopedic, dental and other biomedical applications. It can be used as implants or as coating on implants since it is able to form chemical bonds with living tissue [4,5]. Furthermore, synthetic HAPs have promising applications in drug carrying, protein delivery, growth factor transporter in vitro dissolution, apatite forming ability, antibacterial activity or in vitro cytotoxicity [6–11].

Numerous studies demonstrated the significance and benefits of ion-substitutions in the crystal structure of synthetic HAP. Both cationic (Ag^+ , Mg^{2+} , Sr^{2+} , Zn^{2+} ,) and anionic (CO_3^{2-} , F^- , silicate) substituents can be incorporated to some degree into HAP to replace the calcium or phosphate and hydroxyl groups, respectively. These ion incorporations produce modifications in many physical properties due to the different ionic radii, such as crystallinity, crystallite size, lattice parameters, morphology or even in thermal stability

and solubility [2,12–17]. Additionally, these substitutions can develop or enhance certain characteristics of HAP which improve its biological response and make it more favorable for medical applications. E.g. Ag⁺-substitution results unique antibacterial activity and makes it suitable for bone repair based on in vitro studies [13,17–20]. Besides Ag⁺, other ions, such as Mg²⁺, Sr²⁺ and Zn²⁺-incorporations also evolve the antibacterial activity of the substituted HAPs [21–23]. Furthermore, with Mg- or Sr-substitutions the biocompatibility and osteoconductivity of HAP can be also improved [2,13,14,17,22].

In this study, we prepared pure, Sr- and Mg-substituted HAP samples by precipitation method, using molar ratio 1.67 for Ca/P, (Ca+Sr)/P and (Ca+Mg)/P in accordance with the HAP stoichiometry. After all the preparations, we conducted a 900 °C annealing to improve the crystallinity of the samples. The reaction products were analyzed by XRD, SEM and EDX. Since the effective ion incorporation generates changes in the crystal structure due to the different ionic radii, we determined the lattice parameters and crystallite sizes of the products. As the ionic radius of Ca²⁺ is 0.99Å, but it is 1.12 Å for Sr²⁺ and 0.72 Å for Mg²⁺, enlargement or shrinkage of unit cell, respectively, is expectable.

Finally, we tested the antibacterial activity of the pure and substituted HAPs by microdilution and tetrazolium reduction assay.

2. Experimental

2.1. Preparation of pure and Sr-doped HAP

The synthesis of pure and Sr-doped HAP was carried out by the precipitation method. 0.3 M calcium nitrate tetrahydrate [Ca(NO₃)₂·4H₂O, Sigma Aldrich] solution (A) and 0.29 M

diammonium hydrogen phosphate $[(\text{NH}_4)_2\text{HPO}_4]$, Sigma Aldrich] solution (**B**) were prepared separately in such an amount to keep the molar ratio of Ca/P or (Ca+Sr)/P at 1.67 (**Table 1**). When producing Sr-doped HAP, $\text{Sr}(\text{NO}_3)_2$ (Sigma Aldrich) as Sr source was used together with $\text{Ca}(\text{NO}_3)_2$ for **A**. Subsequently, **B** was added dropwise to **A** under constant stirring, and white precipitate formed immediately. Then the pH was set by NH_4OH (25 %) to 11 and the whole mixture was stirred for 24 hours at room temperature. Finally, the precipitate was collected by filtering, washed with ion-exchanged water and dried at 80 °C for 12 hours.

For investigating the effect of calcination we calcined the samples for 1 h at 900 °C.

The performed experiments are summarized in **Table 1**. First, we studied the effect of calcination at 900 °C for 1 h. After that we carried out Sr-doping with 2, 4, 6, 8 and 12 mol% (SrHAP2, SrHAP4, SrHAP6, SrHAP8, and SrHAP12, respectively). HAP_{rt} means at room temperature-prepared HAP while HAP_{ht} means annealed HAP at 900 °C.

2.2. Preparation of pure and Mg-doped HAP

$\text{Ca}(\text{NO}_3)_2 \cdot 4\text{H}_2\text{O}$ (**C**) and $(\text{NH}_4)_2\text{HPO}_4$ (**D**) solutions were made with the concentration of 0.3 M and 0.29 M, respectively. The Mg source was magnesium nitrate $[\text{Mg}(\text{NO}_3)_2 \cdot 6\text{H}_2\text{O}]$, Sigma Aldrich], which was applied beside $\text{Ca}(\text{NO}_3)_2$ in **C**. In every case the molar ratio of Ca/P or (Ca+Mg)/P was 1.67 (**Table 2**). After that, **D** was added gradually to **C**, which was followed by formation of white precipitate. Subsequently, the mixed solution was stirred for 5 h at 90 °C and then left for aging for 3 days. Finally, it was filtered, washed with ion-exchanged water and dried at 120 °C for 12 h, and calcined at 900 °C for 2 h.

All details of the conducted experiments are in **Table 2**. First, pure HAP was synthesized (HAP90) and then Mg-doped HAP with 2 and 4 mol% of Mg/(Ca+Mg) (MgHAP2, MgHAP4).

HAP90 means the pure HAP prepared applying 90 °C string and 3 days aging.

2.3. Characterization

XRD measurements were carried out by a PANalytical X'Pert Pro MPD diffractometer with Cu K α radiation ($\lambda=0.15418$ nm). To demonstrate the ion incorporation, we carried out lattice parameter calculation using HighScore Plus powder diffraction software. The statistically significant difference between the lattice parameters of pure and doped HAPs was proved by F t-test. Crystallite sizes of the products was evaluated based on the XRD patterns using the Scherrer-formula: $D = \frac{k\lambda}{\beta_m \cos\theta}$, where D (Å) is the crystallite size, k is a unitless form factor (0.9), λ is the wavelength used of the X-ray source (1.5418 Å), β is the physical broadening of the line (full width at half maximum), and θ (rad) is the diffraction angle. The (002) and (310) HA reflections were chosen for the analysis of line broadening along the c-axis and along a direction perpendicular to it, respectively. For investigating the morphology of the obtained materials a LEO 1540 XB electron microscope while for EDX measurements a JEOL JSM 5500-LV instrument was applied.

2.4. Antibacterial activity and *in vitro* cytotoxicity testing

The antibacterial activity and *in vitro* cytotoxicity of pure and Sr-, Mg-doped HAP samples were determined by microdilution method and tetrazolium reduction assay.

Antibacterial tests were carried out against two Gram-negative (*Escherichia coli* ATCC 25922 (American Type Culture Collection) and *Klebsiella pneumoniae* ATCC 49619)

and three Gram-positive bacteria species (*Enterococcus faecalis* ATCC 29212, *Staphylococcus aureus* ATCC 25923, *S. epidermidis* ATCC 29212). The bacteria were prepared in MH (Mueller-Hinton; VWR) broth and were incubated at 37 °C overnight. The assays were performed in 96-well microtiter plates, using a two-fold serial dilution of the HAP samples starting from 200 µg/ml. 10⁻⁴ dilution of an overnight bacterial culture in 100 µL of MH were then added to each well with the exception of the medium control wells. Then, the plates were incubated at 37 °C for 18 h and at the end of the incubation period the MIC values of tested compounds were determined by naked eyes.

In order to investigate whether the different types of pure and substituted HAPs affect the cell viability, the tetrazolium reduction assay was applied using 2-(p-iodophenyl)-3-(p-nitrophenyl)-5-phenyl tetrazolium chloride (INT). In the presence of bacteria, the tetrazolium salt (INT) is reduced to red formazan, which is directly proportional to the viable active cells.

The antibacterial activity test on *Escherichia coli* ATCC 25922 was carried out by direct contact method in shaken tubes with 10 mL of volume Luria-Bertani Broth inoculated with 100-100 µL overnight *E. coli* suspension. The antimicrobial activity of HAP samples was determined at 500 µg/mL and 1 500 µg/mL concentrations in 3-3 parallels after 24 and 48 h incubation time. Control samples without HAPs were also applied in 5 parallels. After 24 and 48 h contact time 200-200 µL of sample was taken out from each tubes and pipetted into 96-well microtiter plate. The optical density (OD) was registered and quantity of formazan was measured after addition of 30 µL sterile INT solution to each cells by recording changes in absorbance at 490 nm using a DIALAB ELx800 ELISA microplate reader. One-way analysis of variance (ANOVA) was performed by STATISTICA 13.1® software identifying significant effects ($p < 0.05$).

3. Results and discussion

3.1. XRD

3.1.1. Effect of calcination

For investigating the role of calcination we applied a 1 h treatment at 900 °C after the precipitation procedure using the undoped sample. HAPrt prepared without calcination and HAPht calcined at 900 °C were both composed of pure HAP (ICDD: 04-016-1647) but with different crystallinity (**Fig. 1**). HAPht has much sharper and narrower peaks, which refers to that HAPht has a more considerably crystallized structure due to the calcination at 900 °C. Since this annealing step does not change the crystalline phase of the prepared samples but improves their crystallinity, at every further preparation it was employed.

3.1.2. Sr-doped HAPs

Sr-doping of HAP was carried out with different Sr/(Ca+Sr) molar ratios. SrHAP2, SrHAP4 were indicated as pure HAP (ICDD: 04-016-1647) without any new peaks referring to the Sr-content (**Fig.2**). The peak positions of SrHAP2 and SrHAP4 slightly shifted towards lower diffraction angles from 31.848 2 θ (HAPht) to 31.784 2 θ and 31.705 2 θ , respectively, in the case of the most intensive peak (310). Based on the results, it was assumed that Sr ions incorporated into the unit cell of HAP substituting Ca ions. In the case of SrHAP6, SrHAP8 and SrHAP12 Sr-containing tricalcium phosphate ($\text{Sr}_{0.13}\text{Ca}_{2.87}(\text{PO}_4)_2$, ICDD: 04-015-9751) and calcium pyrophosphate ($\text{Ca}_2\text{P}_2\text{O}_7$, ICDD: 04-009-3876) phases were determined. The lack of HAP is due to the distortion effect of Sr on the phosphate environment, which promotes the decomposition of HAP at high

temperatures [24,25] and the transformation of HAP to β -TCP (tricalcium phosphate) above 700 °C. [26,27]

The HAPht results are in good agreement with the ones in the reference pattern (ICDD: 01-082-2956), which are a, b (Å) = 9.4154, c (Å): 6.8792 and V (Å³) = 528.14. The calculated lattice parameters obtained from the XRD patterns for the pure and Sr-doped HAPs (HAPht-SrHAP2-SrHAP4) altered slightly due to the larger ionic radius of Sr²⁺ (1.12 Å) compared to Ca²⁺ (0.99 Å, **Table 3**). Parameters a and b changed from 9.4100 to 9.4266 Å, c from 6.8753 to 6.8925 Å, while the volume of unit cell expanded from 527.22 to 530.41 Å³. In the case of the doped samples (SrHAP2 and SrHAP4) it is clearly seen that all the parameters (a, b, c) and volume of the unit cell increased. This effect is attributed to the Sr incorporation into the structure of HAP which substitutes Ca ions and thus expands the unit cell. In the terms of the crystallite sizes calculated by the Scherrer-formula, a significant increase is present. The FWHM values used for the calculation decreased meaning the growth of the crystallite size, which can occur to some Sr content [28,29]. The lattice parameters of SrHAP2 and SrHAP4 differed significantly compared to pure HAP based on statistical calculation (F and t probes).

3.1.3. Mg-doped HAPs

Based on the XRD patterns, HAP90 and MgHAP2 were identified as pure HAP (ICDD: 04-016-1647) and no other Mg-containing phase obtained (**Fig.3**). The peaks were supposed to be at higher diffraction angles indicating the shrinkage of unit cell, however, the positions for the most intensive peak were 31.776 2 θ and 31.761 2 θ in HAP90 and MgHAP2, respectively. When applying 4 % Mg, Mg and Ca-containing phase of triphosphate was also identified (Ca_{2.71}Mg_{0.29}(PO₄)₂, ICDD: 04-010-2972). The results

show that starting from 4 % concentration Mg was not able to build into the crystal structure of HAP owing to the destabilizing influence of Mg. [30,31]

Table 4 shows the calculated lattice parameters of HAP90 and MgHAP2. The obtained values for HAP90 correspond the ones from the reference HAP pattern (ICDD: 01-082-2956), which are a, b (Å) = 9.4154, c (Å): 6.8792 and V (Å³) = 528.14. We expected a slight decrease in the values as the ionic radius of Mg²⁺ is smaller (0.72 Å) than Ca²⁺ (0.99 Å). Parameter a and b were 9.4137 Å and 9.4124 Å for HAP90 and MgHAP2, respectively. Even the volume of unit cell decreased from 527.73 Å³ to 527.63 Å³. However, parameter c was 6.8764 Å for HAP90 and 6.8771 Å for MgHAP2, which means some distortion of the unit cell. The crystallite sizes got larger in the presence of 2 % Mg, which was obvious due to the narrower FWHM values used for the calculation. The difference between a, b lattice parameters of MgHAP2 was significant compared to HAP90 based on statistical calculation (F and t probes).

3.2. EDX

Our main purpose with the EDX was to directly detect the presence of the doping ions. The lattice parameter calculations revealed changes in the unit cells referring to the incorporation but the ions are expected to be detected by EDX as well.

3.2.1. Sr-doped HAPs

Ca, Sr, P and O elements were the main components in each sample. This indicates that the washing process after filtering was sufficient as N was not observed during the measurements. **Table 5** presents that the Ca/P or (Ca+Sr)/P molar ratios are approximately 1.67 in the case of HAPht and SrHAP4 but only 1.42 for SrHAP2. This small ratio would mean the formation of Ca-deficient HAP which decomposes above 700

°C to β -TCP [26,27,32]. As the samples were pure HAP without any other phases, we assume the real value is close to the theoretical 1.67. For the same reason, the discrepancies in Sr/(Ca+Sr) ratios (1.71 for SrHAP2, 2.71 for SrHAP4) is attributed to the non-accuracy of EDX for quantitative analysis. In the case of SrHAP6, SrHAP8 and SrHAP12 the decrease of measured Sr % is according to the formation of new phases ($\text{Sr}_x\text{Ca}_{3-x}(\text{PO}_4)_2$, $\text{Ca}_2\text{P}_2\text{O}_7$, **Table 5**, Fig.S1).

3.2.2. Mg-doped HAPs

HAP90, MgHAP2 and MgHAP4 consisted of only Ca, Mg, P and O (**Table 6**, Fig. S2). N was not detectable, which is in good agreement with the XRD results, where pure HAP (HAP90, MgHAP2) and $\text{Mg}_{0.29}\text{Ca}_{2.71}(\text{PO}_4)_2$ (MgHAP4) were identified. We conclude that the Ca/P and (Ca+Mg)/P atomic ratios were 1.67 at each sample, since according to the XRD results MgHAP2 has composed of only HAP. The measured Mg/(Ca+Mg) ratios is considered closing the planned 2 and 4 %. In the case of MgHAP4 the difference is attributed to formation not only HAP but a new phase.

3.3. Morphology

In the SEM image of HAPht nanometer sized grains are observable, which are highly sintered (**Fig.4**). In the case of SrHAP2 and SrHAP4 formation of elongated shapes, similar to HAPht, can be seen. The sintered forms have dimensions of 100-200 nm and are strongly stacked to each other. According to them, the incorporation of Sr-ion into the crystal structure of HAP does not change the morphology significantly.

In the case of SrHAP6, SrHAP8, SrHAP12 the samples were composed of larger crystals with various shapes and sizes (more than 500 nm, **Fig.4**). This effect is due to the fact

that in these experiments not HAP but other phases ($\text{Sr}_{0.13}\text{Ca}_{2.87}(\text{PO}_4)_2$, $(\text{Ca}_2\text{P}_2\text{O}_7)$) were formed.

In the SEM images of HAP90, MgHAP2 and MgHAP4 (**Fig.5**) it can be detected that the morphology of the samples are homogenous and consist of mostly some roundish forms, however, with different sizes. In the case of MgHAP2 these forms are in the range of 400-500 nm while in MgHAP4 they are 100-200 nm compared to HAP90. HAP90 is composed of mostly 300 nm rounded grains.

3.4. Antibacterial activity and *in vitro* cytotoxicity testing

Testing of the antibacterial activity and *in vitro* cytotoxicity of the pure, Sr- and Mg-doped HAP samples was carried out by determination MIC values using microdilution and INT reduction method.

Based on the results of the microdilution method, MgHAP2 had effect on inhibiting the growth of both Gram-positive and negative strains compared to pure HAP (**Table 7**). In the case of SrHAP2 and SrHAP4 this effect can occur at more than 200 $\mu\text{g/ml}$ concentrations.

According to the results of INT reduction, SrHAP4 was effective against *E. coli* as the absorbance was decreased at both applied concentration. Statistically significant decrease (~26% inhibition) was observed at 1500 $\mu\text{g/ml}$ SrHAP4. Slight but not significant antibacterial activity (~10% inhibition) was found in the case of MgHAP2 compared to control (**Fig. 6**).

4. Conclusion

In this study we synthesized pure HAP by precipitation method and incorporated Sr and Mg-ions into its crystal lattice. We applied different molar ratios: 2, 4, 6, 8 and 12 Sr/(Ca+Sr) mol% and 2, 4 Mg/ (Ca+Mg) mol%. Based on the XRD measurements we found that SrHAP2 and SrHAP4 had pure crystalline HAP structure and the EDX experiments definitely showed Sr content. The same happened at in MgHAP2 which was identified pure HAP and EDX detected Mg presence. The other samples, prepared with different molar ratios of Sr and Mg, consisted of $\text{Sr}_{0.13}\text{Ca}_{2.87}(\text{PO}_4)_2$, $\text{Ca}_2\text{P}_2\text{O}_7$, $\text{Mg}_{0.29}\text{Ca}_{2.71}(\text{PO}_4)_2$. The ion incorporation into the crystalline hexagonal structure of HAP induced changes in the parameters and volume of the unit cell, moreover in the crystallite size. Since the bigger ionic radius of Sr^{2+} to Ca^{2+} in SrHAP2 and SrHAP4 the unit cell of HAP expanded confirmed by the increasing of parameter a (b), c and the volume of unit cell. As the ionic radius of Mg^{2+} is smaller than Ca^{2+} , we demonstrated that a (b) parameters and unit cell volume decreased. Parameter c was however increased, which refers unit cell distortion. Crystallite sizes increased when the amount of Sr and Mg was higher as a consequence of the narrower XRD reflections compared to the pure HAPs. SEM images showed that every sample had homogenous morphology, with elongated and roundish shapes strongly stacked to each other. These forms were 100-200 nm wide in the case of 2 and 4 % Sr but at higher amounts of Sr they were larger (400-500 nm). 2 % Mg HAP resulted larger roundish crystals than in the case of 4 % Mg. Results of antimicrobial experiments showed that in the case of MgHAP2 sample the MIC value was 100 $\mu\text{g}/\text{ml}$, however, more than 200 $\mu\text{g}/\text{ml}$ for the Sr-doped HAPs on the tested strains. For *in vitro* cytotoxicity tests only SrHAP4 had influence on the reduction of INT compared to the pure sample at 1500 $\mu\text{g}/\text{ml}$, MgHAP2 revealed slight differences.

5. Associated content

Supporting Information. EDX spectra of HAPht, SrHAP2, SrHAP4, SrHAP6, SrHAP8 and SrHAP12 (Fig.S1) and EDX spectra of HAP90, MgHAP2 and MgHAP4 (Fig.S2).

6. Acknowledgements

T. Nagyné-Kovács thanks for an ÚNKP-17-3-I-BME-192 grant supported by the ÚNKP-17-3-I New National Excellence Program of the Ministry of Human Capacities, Hungary. I. M. Szilágyi thanks for a János Bolyai Research Fellowship of the Hungarian Academy of Sciences and an ÚNKP-17-4-IV-BME-188 grant supported by the ÚNKP-17-4-IV New National Excellence Program of the Ministry of Human Capacities, Hungary. An NRD K 124212 and an NRD TNN_16 123631 grant are acknowledged. The research within project No. VEKOP-2.3.2-16-2017-00013 was supported by the European Union and the State of Hungary, co-financed by the European Regional Development Fund. The research reported in this paper was supported by the Higher Education Excellence Program of the Ministry of Human Capacities in the frame of Nanotechnology and Materials Science research area of Budapest University of Technology (BME FIKP-NAT).

References

- [1] C. Combes, S. Cazalbou, C. Rey, *Apatite Biominerals*, *Minerals*. 6 (2016) 34.
doi:10.3390/min6020034.
- [2] J.T.B. Ratnayake, M. Mucalo, G.J. Dias, *Substituted hydroxyapatites for bone regeneration: A review of current trends*, *J. Biomed. Mater. Res. - Part B Appl. Biomater.* 105 (2017) 1285–1299. doi:10.1002/jbm.b.33651.
- [3] P.. Downey, M. Siegel, *Bone Biology and the Clinical Implications for osteoporosis*, *Phys. Ther.* 86 (2006) 77–91.
- [4] T. Inadome, K. Hayashi, Y. Nakashima, H. Tsumura, Y. Sugioka, *Comparison of bone implant interface shear strength of hydroxyapatite-coated and alumina-coated metal implants*, *J. Biomed. Mater. Res.* 29 (1995) 19–24. doi:10.1002/jbm.820290104.
- [5] K. Søballe, E.S. Hansen, H. B.-Rasmussen, P.H. Jørgensen, C. Bünger, *Tissue ingrowth into titanium and hydroxyapatite-coated implants during stable and unstable mechanical conditions*, *J. Orthop. Res.* 10 (1992) 285–299. doi:10.1002/jor.1100100216.
- [6] M. Okada, T. Furuzono, *Hydroxylapatite nanoparticles: Fabrication methods and medical applications*, *Sci. Technol. Adv. Mater.* 13 (2012). doi:10.1088/1468-6996/13/6/064103.
- [7] C. Shi, J. Gao, M. Wang, J. Fu, D. Wang, Y. Zhu, *Ultra-trace silver-doped hydroxyapatite with non-cytotoxicity and effective antibacterial activity*, *Mater. Sci. Eng. C.* 55 (2015) 497–505. doi:10.1016/j.msec.2015.05.078.
- [8] N. Ohtsu, Y. Kakuchi, T. Ohtsuki, *Antibacterial effect of zinc oxide/hydroxyapatite coatings prepared by chemical solution deposition*, *Appl. Surf. Sci.* (2017).
doi:10.1016/j.apsusc.2017.09.101.
- [9] G.S. Kumar, A. Thamizhavel, Y. Yokogawa, S.N. Kalkura, E.K. Girija, *Synthesis,*

- characterization and in vitro studies of zinc and carbonate co-substituted nano-hydroxyapatite for biomedical applications, *Mater. Chem. Phys.* 134 (2012) 1127–1135.
doi:10.1016/j.matchemphys.2012.04.005.
- [10] K. Lin, P. Liu, L. Wei, Z. Zou, W. Zhang, Y. Qian, Y. Shen, J. Chang, Strontium substituted hydroxyapatite porous microspheres: Surfactant-free hydrothermal synthesis, enhanced biological response and sustained drug release, *Chem. Eng. J.* 222 (2013) 49–59. doi:10.1016/j.cej.2013.02.037.
- [11] D. Gopi, E. Shinyjoy, L. Kavitha, Synthesis and spectral characterization of silver/magnesium co-substituted hydroxyapatite for biomedical applications, *Spectrochim. Acta - Part A Mol. Biomol. Spectrosc.* 127 (2014) 286–291.
doi:10.1016/j.saa.2014.02.057.
- [12] F. Miyaji, Y. Kono, Y. Suyama, Formation and structure of zinc-substituted calcium hydroxyapatite, *Mater. Res. Bull.* 40 (2005) 209–220.
doi:10.1016/j.materresbull.2004.10.020.
- [13] K.T. Arul, J.R. Ramya, G.M. Bhalerao, S.N. Kalkura, Physicochemical characterization of the superhydrophilic, magnesium and silver ions co-incorporated nanocrystalline hydroxyapatite, synthesized by microwave processing, *Ceram. Int.* 40 (2014) 13771–13779. doi:10.1016/j.ceramint.2014.05.088.
- [14] A. Bigi, E. Boanini, C. Capuccini, M. Gazzano, Strontium-substituted hydroxyapatite nanocrystals, *Inorganica Chim. Acta.* 360 (2007) 1009–1016.
doi:10.1016/j.ica.2006.07.074.
- [15] N. Lowry, Y. Han, B.J. Meenan, A.R. Boyd, Strontium and zinc co-substituted nanophase hydroxyapatite, *Ceram. Int.* 43 (2017) 12070–12078.
doi:10.1016/j.ceramint.2017.06.062.

- [16] N. Patel, S.M. Best, W. Bonfield, I.R. Gibson, K.A. Hing, E. Damien, P.A. Revell, A comparative study on the in vivo behavior of hydroxyapatite and silicon substituted hydroxyapatite granules, *J. Mater. Sci. Mater. Med.* 13 (2002) 1199–1206. doi:10.1023/A:1021114710076.
- [17] J.H. Shepherd, D. V. Shepherd, S.M. Best, Substituted hydroxyapatites for bone repair, *J. Mater. Sci. Mater. Med.* 23 (2012) 2335–2347. doi:10.1007/s10856-012-4598-2.
- [18] P.N. Lim, E.Y. Teo, B. Ho, B.Y. Tay, E.S. Thian, Effect of silver content on the antibacterial and bioactive properties of silver-substituted hydroxyapatite, *J. Biomed. Mater. Res. - Part A.* 101 A (2013) 2456–2464. doi:10.1002/jbm.a.34544.
- [19] T.N. Kim, Q.L. Feng, J.O. Kim, J. Wu, H. Wang, G.C. Chen, F.Z. Cui, Antimicrobial effects of metal ions (Ag⁺, Cu²⁺, Zn²⁺) in hydroxyapatite, *J. Mater. Sci. Mater. Med.* 9 (1998) 129–134. doi:10.1023/A:1008811501734.
- [20] A. Ewald, D. Hösel, S. Patel, L.M. Grover, J.E. Barralet, U. Gbureck, Silver-doped calcium phosphate cements with antimicrobial activity, *Acta Biomater.* 7 (2011) 4064–4070. doi:10.1016/j.actbio.2011.06.049.
- [21] A. Farzadi, F. Bakhshi, M. Solati-Hashjin, M. Asadi-Eydivand, N.A.A. Osman, Magnesium incorporated hydroxyapatite: Synthesis and structural properties characterization, *Ceram. Int.* 40 (2014) 6021–6029. doi:10.1016/j.ceramint.2013.11.051.
- [22] N.D. Ravi, R. Balu, T.S. Sampath Kumar, Strontium-substituted calcium deficient hydroxyapatite nanoparticles: Synthesis, characterization, and antibacterial properties, *J. Am. Ceram. Soc.* 95 (2012) 2700–2708. doi:10.1111/j.1551-2916.2012.05262.x.
- [23] V. Stanić, S. Dimitrijević, J. Antić-Stanković, M. Mitrić, B. Jokić, I.B. Plećaš, S. Raičević, Synthesis, characterization and antimicrobial activity of copper and zinc-doped hydroxyapatite nanopowders, *Appl. Surf. Sci.* 256 (2010) 6083–6089.

doi:10.1016/j.apsusc.2010.03.124.

- [24] Z.Y. Li, W.M. Lam, C. Yang, B. Xu, G.X. Ni, S.A. Abbah, K.M.C. Cheung, K.D.K. Luk, W.W. Lu, Chemical composition, crystal size and lattice structural changes after incorporation of strontium into biomimetic apatite, *Biomaterials*. 28 (2007) 1452–1460. doi:10.1016/j.biomaterials.2006.11.001.
- [25] H.W. Kim, Y.H. Koh, Y.M. Kong, J.G. Kang, H.E. Kim, Strontium substituted calcium phosphate biphasic ceramics obtained by a powder precipitation method, *J. Mater. Sci. Mater. Med.* 15 (2004) 1129–1134. doi:10.1023/B:JMSM.0000046395.76435.60.
- [26] I.R. Gibson, I. Rehman, S.M. Best, W. Bonfield, Characterization of the transformation from calcium-deficient apatite to β -tricalcium phosphate, *J. Mater. Sci. Mater. Med.* 11 (2000) 799–804. doi:10.1023/A:1008905613182.
- [27] D. dos S. Tavares, C.X. Resende, M.P. Quitan, L. de O. Castro, J.M. Granjeiro, G. de A. Soares, Incorporation of strontium up to 5 Mol. (%) to hydroxyapatite did not affect its cytocompatibility, *Mater. Res.* 14 (2011) 456–460. doi:10.1590/S1516-14392011005000073.
- [28] P.H. RABELO NETO, J. S.; KNOPF, T. B.; FREDEL, M. C.; OLATE, S. & DE MORAES, Synthesis and Characterization of Calcium Phosphate Compounds with Strontium and Magnesium Ionic Substitutions, *Int. J. Morphol.* 33 (2015) 1189–1193. doi:10.4067/S0717-95022015000300061.
- [29] R. V Suganthi, K. Elayaraja, M.I.A. Joshy, V.S. Chandra, E.K. Girija, S.N. Kalkura, Fibrous growth of strontium substituted hydroxyapatite and its drug release, *Mater. Sci. Eng. C*. 31 (2011) 593–599. doi:10.1016/j.msec.2010.11.025.
- [30] A. Bigi, G. Falini, E. Foresti, A. Ripamonti, M. Gazzano, N. Roveri, Magnesium influence on hydroxyapatite crystallization, *J. Inorg. Biochem.* 49 (1993) 69–78.

doi:10.1016/0162-0134(93)80049-F.

- [31] F. Ren, Y. Leng, R. Xin, X. Ge, Synthesis, characterization and ab initio simulation of magnesium-substituted hydroxyapatite, *Acta Biomater.* 6 (2010) 2787–2796.

doi:10.1016/j.actbio.2009.12.044.

- [32] L. Leroux, J.L. Lacout, Preparation of calcium strontium hydroxyapatites by a new route involving calcium phosphate cements, *J. Mater. Res.* 16 (2001) 171–178.

doi:10.1557/JMR.2001.0028.

Table and figure captions

Table 1 Details of the preparation of pure and Sr-doped HAP

Table 2 Details of the preparation of pure and Mg-doped HAP

Table 3 Calculated lattice parameters of HAP_{ht}, SrHAP₂ and SrHAP₄

Table 4 Calculated lattice parameters of HAP₉₀ and MgHAP₂

Table 5 EDX results of pure and Sr-doped HAPs

Table 6 EDX results of pure and Mg-doped HAPs

Table 7 Results of MIC determination by microdilution method

Figure 1 XRD patterns of HAP_{rt} and HAP_{ht}

Figure 2 XRD patterns of pure and Sr-doped HAPs

Figure 3 XRD patterns of pure and Mg-doped HAPs

Figure 4 SEM images of pure and Sr-doped HAPs

Figure 5 SEM images of pure and Mg-doped HAPs

Figure 6 Tetrazolium (INT) reduction results for pure and doped HAP samples

Table 7

	HAPrt	HAPht	SrHAP2	SrHAP4	SrHAP6	SrHAP8	SrHAP12
Sr/(Ca+Sr) [mol%]	0	0	2	4	6	8	12
(Sr+Ca)/P	1.67	1.67	1.67	1.67	1.67	1.67	1.67
Ca(NO₃)₂·4H₂O (mol)	0.02030	0.02030	0.01994	0.01953	0.01912	0.01871	0.01790
Sr(NO₃)₂ (mmol)	0	0	0.407	0.814	1.220	1.627	2.440
c_A (M)	0.30	0.30	0.30	0.30	0.30	0.30	0.30
(NH₄)₂HPO₄ (mol)	0.012	0.012	0.012	0.012	0.012	0.012	0.012
c_B (M)	0.29	0.29	0.29	0.29	0.29	0.29	0.29
Calcination (900 °C)	no	yes	yes	yes	yes	yes	yes

Table 8

	HAP90	MgHAP2	MgHAP4
Mg/(Ca+Mg) [mol%]	0	2	4
(Mg+Ca)/P	1.67	1.67	1.67
Ca(NO₃)₂·4H₂O (mol)	0.02	0.0196	0.0192
Mg(NO₃)₂·6 H₂O (mmol)	0	0.4	0.8
cc (M)	0.2	0.2	0.2
(NH₄)₂HPO₄ (mol)	0.012	0.012	0.012
cd (M)	0.12	0.12	0.12
Calcination (900 °C)	yes	yes	yes

Table 9

	Lattice parameters				Crystallite size (nm)	
	a (Å)	b (Å)	c (Å)	V (Å ³)	002	310
HAPht	9.4100	9.4100	6.8753	527.22	48.27	38.26
SrHAP2	9.4189	9.4189	6.8851	528.99	70.94	67.11
SrHAP4	9.4266	9.4266	6.8925	530.41	95.90	62.62

Table 10

	Lattice parameters				Crystallite size (nm)	
	a (Å)	b (Å)	c (Å)	V (Å ³)	002	310
HAP90	9.4137	9.4137	6.8764	527.73	113.37	100.70
MgHAP2	9.4124	9.4124	6.8771	527.63	151.22	176.38

Table 11

	HAPht	SrHAP2	SrHAP4	SrHAP6	SrHAP8	SrHAP12
Ca (atom %)	21.48	14.92	18.34	16.35	13.89	24.92
Sr (atom %)	-	0.26	0.51	0.49	0.78	0.94
P (atom %)	12.93	10.70	11.73	13.31	12.04	14.86
O (atom %)	65.59	74.13	69.41	69.85	73.28	59.28
Ca/P or (Ca+Sr)/P	1.66	1.42	1.61	1.27	1.22	1.74
Sr/(Ca+Sr)	-	1.71	2.71	2.91	5.32	3.63

Table 12

	HAP90	MgHAP2	MgHAP4
Ca (atom %)	22.63	19.92	19.59
Mg (atom %)	-	0.33	0.63
P (atom %)	12.58	12.06	13.26
O (atom %)	64.79	67.68	66.52
Ca/P or (Ca+Mg)/P	1.80	1.68	1.52
Mg/(Ca+Mg)	-	1.63	3.12

Table 7

	HAPht	SrHAP2	SrHAP4	HAP90	MgHAP2
<i>S. aureus</i> ATCC 25923	>200	>200	>200	>200	100
<i>S. epidermidis</i> ATCC 12228	>200	>200	>200	>200	100
<i>E. faecalis</i> ATCC 29212	>200	>200	>200	>200	100
<i>K. pneumoniae</i> ATCC 49619	>200	>200	>200	>200	100
<i>E. coli</i> ATCC 25922	>200	>200	>200	>200	100

Figure 4

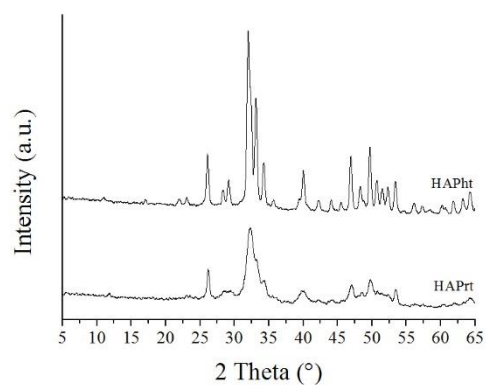


Figure 5

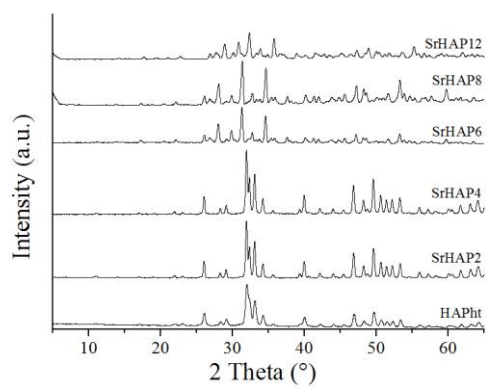


Figure 6

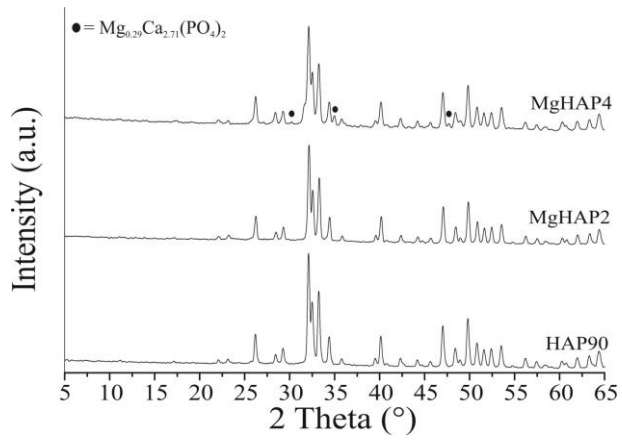


Figure 4

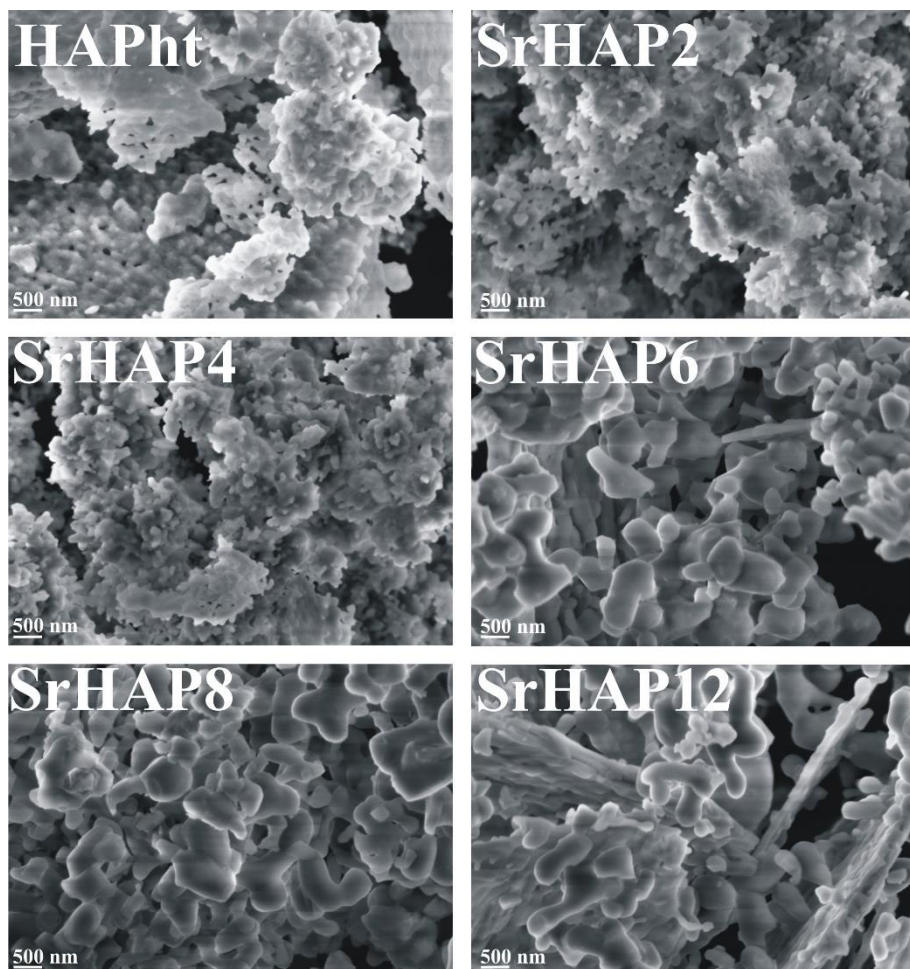


Figure 5

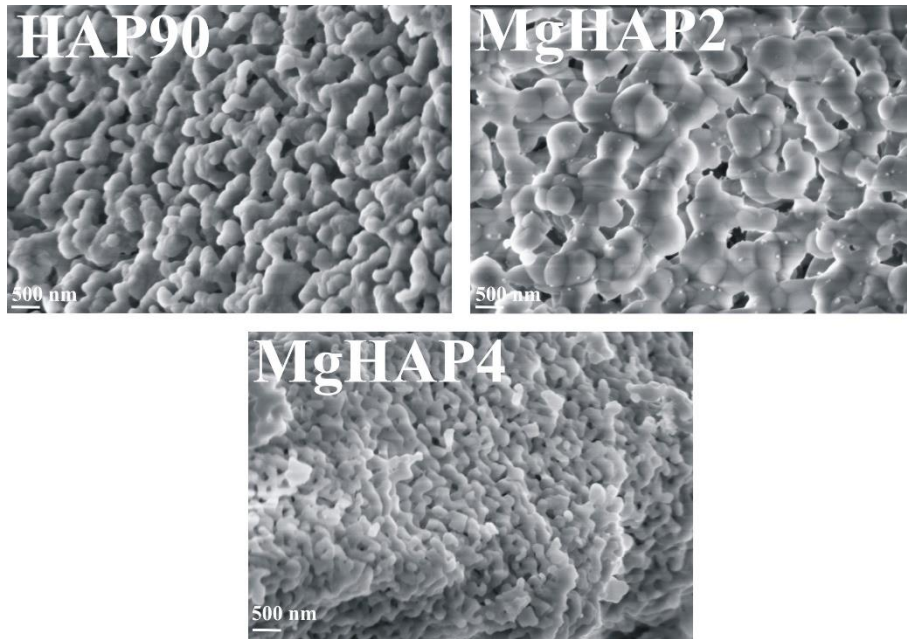


Figure 6

